Journal of New Materials for Electrochemical Systems 20, 197-204 (2017)

Hierarchical Dendritic Polypyrrole with High Specific Capacitance for High-performance Supercapacitor Electrode Materials

Weiliang Chen[1], Shuhua Pang[1], Zheng Liu[1,2], Zhewei Yang[1], Xin Fan[1,*], and Dong Fang[3,†]

[1]Key Laboratory of New Processing Technology for Nonferrous Metal and Materials of Ministry of Education, College of Materials Science & Engineering, Guilin University of Technology, Guilin 541004, China

[2]BengBu Center of Product Quality Supervising & Inspection, BengBu 233000, China

[3]College of Material Science and Engineering, Wuhan Textile University, Wuhan 430700, China

Received: August 20, 2017, Accepted: September 06, 2017, Available online: October 17, 2017

Abstract: *Polypyrrole with hierarchical dendritic structures assembled with cauliflower-like structure of nanospheres, was synthesized by chemical oxidation polymerization. The structure of polyryrrole was characterized by Fourier transform infrared spectrometer and scanning electron microscopy. The electrochemical performance was performed on CHI660 electrochemical workstation. The results show that oxalic acid has a significant effect on morphology of PPy products. The hierarchical dendritic $PPy_{OA(3)}$ electrodes possess a large specific capacitance as high as 744 F/g at a current density of 0.2 A/g and could achieve a higher specific capacitance of 362 F/g even at a current density of 5.0 A/g. Moreover, the dendritic PPy products produce a large surface area on the electrode through the formation of the channel structure with their assembled cauliflower-like morphology, which facilitates the charge/electron transfer relative to the spherical PPy electrode. The spherical dendritic $PPy_{OA(3)}$ electrode has 58% retention of initial specific capacitance after 260 cycles. The as-prepared dendritic polypyrrole with high performance is a promsing electrode material for supercapacitor.*

Keywords: hierarchical dendritic polypyrrole; high-performance; supercapacitor; eletrode material

1. INTRODUCTION

Electrochemical capacitors (ECs or supercapacitors), as promising efficient electrical energy storage devices, have recently received keen interest because of their advantages such as high power density, low maintenance cost and long durability in comparison to batteries and conventional capacitors[1,2]. Further, the investigation into ECs has focused on the high performance of the electrode with high capacitance, high conductivity and excellent electrochemical cycle stability. Recently, conducting polymers, as a type of pseudo-capacitive materials, have attracted great interest on the recent developments in this most exciting field, especially polypyrrole (PPy). PPy, as a kind of traditional conducting polymer[3,4], is promising and has been the subject of much research as a supercapacitor electrode material ascribed to low cost, high pseudocapacitance and controllable electrical conductivity, excellent chemical and good environmental stability, and unique conductive mechanism. Nevertheless, the volume expansion induced by doping and de-doping in electrochemical progress lowers the stability of electrochemical capacitors. PPy is generally fabricated by electrochemical polymerization[5-9], chemical interfacial polymerization[10-12], in situ depositing method[13] or chemical oxidation polymerization[14,15]. Among these approaches, chemical oxidation polymerization is a facile and effective way to synthesize PPy. However, the reported specific capacitances of the PPy are rather low.

As the development of nanoscience, the micro/nanostructure and morphology of electrode material have a significant impact on its electrochemical performance[16]. The electrochemical storage capacity of PPy has been reported varying with its morphology, particle sizes and specific surface areas. And a chemical oxidation polymerization is usually performed in the phase interface or with the help of surfactant to control the final morphology of the conducting polymer[17,18]. Dendrite is a hierarchical structure, which consists of main stems in micrometer size and branches in nanometer size, like a pine-tree structure[19]. Dendritic structure,

To whom correspondence should be addressed:
Email: *xfan@glut.edu.cn, †csufangdong@gmail.com

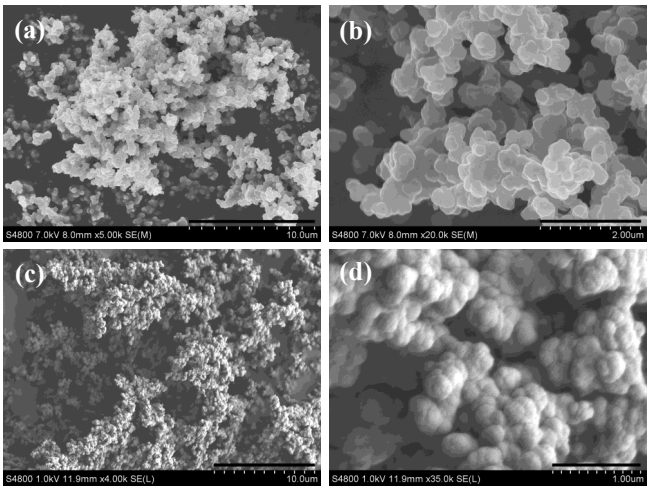

Figure 1. SEM images of (a, b) PPy and (c, d) $PPy_{OA(3)}$ samples. Scale bar (a) 10 μm, (b) 2μm , (c)10μm ,(d) 1μm.

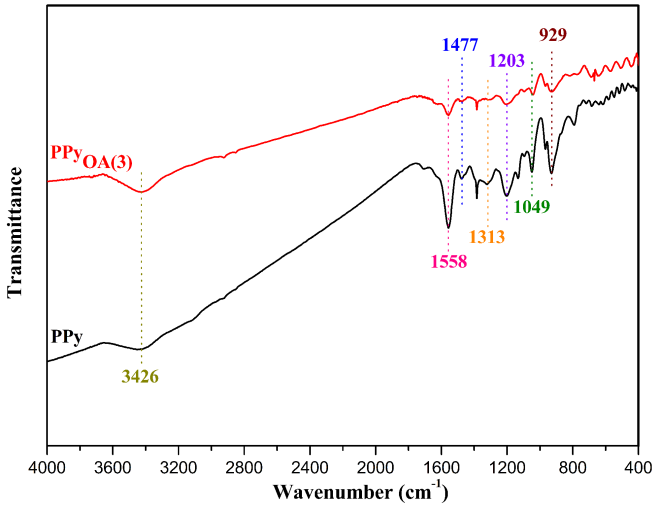

Figure 2. FTIR spectra of PPy and $PPy_{OA(3)}$ samples.

comprising a configured channel for carrying charge and exciton efficiently[20,21], due to its good porous structure and high specific surface area, is ideal building blocks for functional nanoscale devices. Dendritic materials have attracted much attention for potential applications in energy storage sources.

In this work, a hierarchical dendritic micro/nanostructure PPy (denoted as $PPy_{OA(3)}$, molar ratio of oxalic acid/pyrrole = 3) was prepared by chemical oxidation polymerization using oxalic acid as the template and chlorine hydride solution as the doping agent. The structure and morphology of the as-synthesized PPy was characterized and the electrochemical performance for supercapacitor electrode materials was investigated in detail in the following sections.

2. EXPERIMENTAL MATERIALS

2.1. Preparation of hierarchical dendritic PPy

The carbanyl group in oxalic acid facilitates massive pyrrole monomers to gather on the surface of oxalic acid by formed hydrogen bond with -NH in pyrrole ring. Then pyrrole monomers are polymerized on the condition of APS. A typical experiment process is shown as follows.

1.17 mL oxalic acid was dispersed into 50 mL deionized water and stirred for 20 min at room temperature. Then 0.5 mL pyrrole was added into the oxalic acid solution and stirred for 1 h in a ice-water bath to obtain a uniform solution (molar ratio of oxalic acid/pyrrole = 3). Next, 10 mL of 1.6482 g aqueous solution of APS (molar ratio of pyrrole/APS = 1) was drop by drop added into the reaction mixture under vigorous stirring in a ice-water bath for 8 h. Finally, the products were filtered and washed with deionized water and ethanol repeatedly until the filtrate was neutral, and dried in a vacuum oven at 60 ºC for 24 h. The resultant products were denoted $PPy_{OA(3)}$.

For comparison, the PPy products prepared without the presence of oxalic acid and at different molar ratios of oxalic acid/pyrrole (1, 1/3, 1/5, 1/10) by the same method were denoted as PPy, $PPy_{OA(1)}$, $PPy_{OA(1/3)}$, $PPy_{OA(1/5)}$ and $PPy_{OA(1/10)}$.

2.2. Material characterization

FTIR was carried out on Fourier transform infrared spectrometer (Thermo Nexus 470 FT-IR). Scanning electron microscopy (SEM) was performed on a Hitachi S4800 FESEM.

2.3. Electrode preparation and electrochemical test

The electrochemical measurements were performed on CHI690 electrochemical workstation in an electrolyte of 1 M H_2SO_4 solution, using platinum foil as a counter electrode and saturated calomel electrode as a reference electrode by cyclic voltammetry (CV), galvanostatic charge-discharge (GCD) and electrochemical impedance spectroscopy (EIS) experiments. The specific capacitance of the electrode was measured by GCD and could be calculated according to the following equation:

$$C_s=(I\cdot\Delta t)/(\Delta V\cdot m) \quad (1)$$

where I is the current, Δt is the discharge time, m is total mass of active material in a single electrode, and ΔV is the potential window.

The working electrode was prepared by sufficient mixing the composite, conductive black and polytetrafluor-ethylene (mass ratio=8:1:1), yielding homogeneous slurry under ultrasonic dispersion. The slurry was coated and pressed onto stainless steel wire (the area is 1 cm^2 and the mass of active material was about 5~10 mg), then dried in a vacuum oven at 60 ºC for 24 h[24].

EIS test was performed at a temprature of 25 ºC. The initial potential is the open curcuit potential, frequecy range is 0.01~10^5 Hz, and amplititude is 5 mV.

3. RESULTS AND DISCUSSION

3.1. Materials structure analysis

The morphologies of the as-prepared PPy and $PPy_{OA(3)}$ powder were investigated using SEM (Fig. 1). We find that PPy shows ball-like sphere, randomly scattering and partially stacking together with each other (Fig. 1a and b), and $PPy_{OA(3)}$ exhibited hierarchical dendritic structures assembled with cauliflower-like structure of

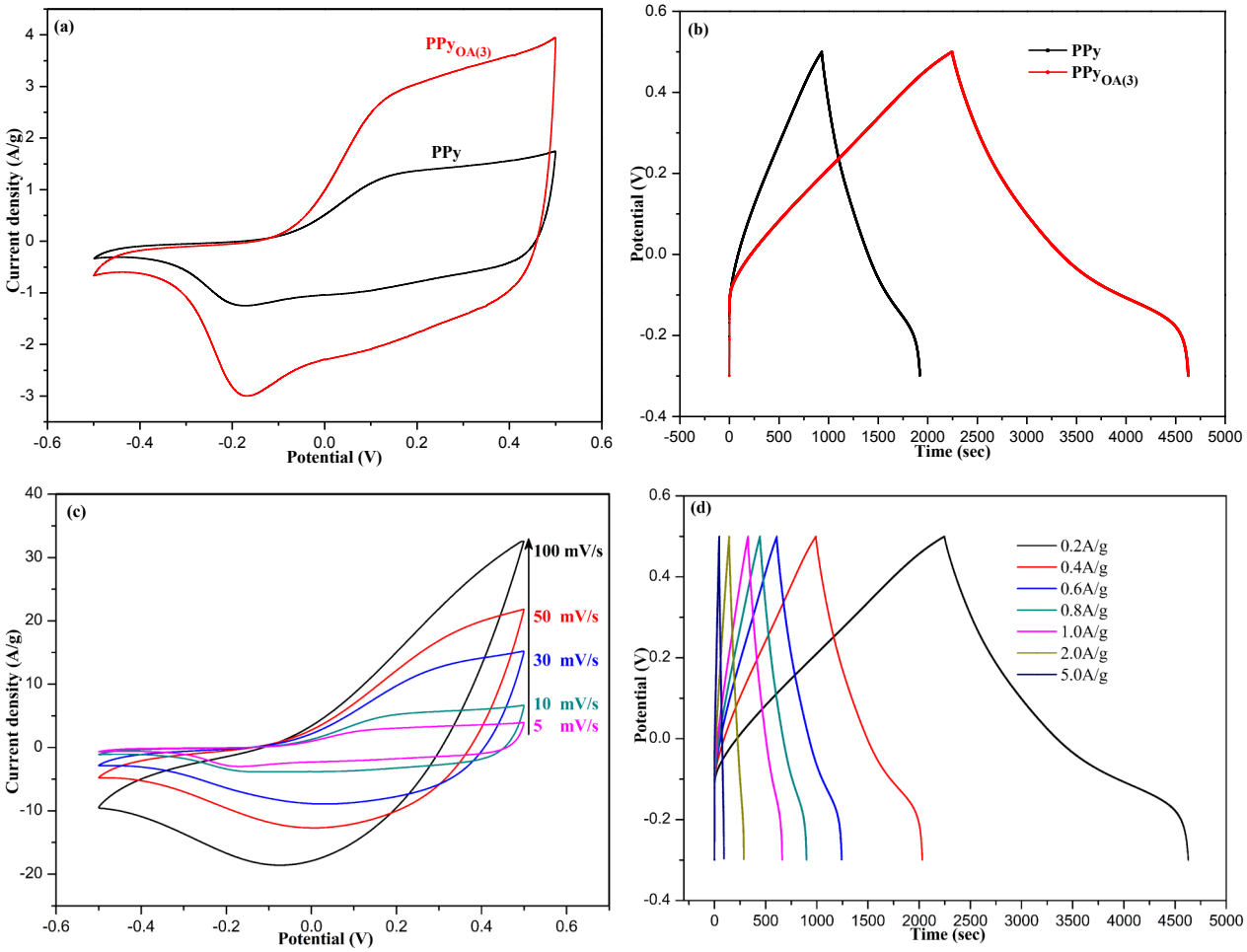

Figure 3. (a) CV curves of PPy and PPy$_{OA(3)}$ samples at scan rate of 5 mV/s; (b) GCD curves of PPy and PPy$_{OA(3)}$ samples at current density of 0.2 A/g; (c) CV curves of PPy$_{OA(3)}$ at various scan rates; (d) GCD curves of PPy$_{OA(3)}$ at various current densities. (vs. SCE)

nanospheres, which seemed to share a common trunk and grow outwards along the radial direction (Fig. 1c and d). This cauliflower-like structure is mainly related to the doping difficulty in the disordered polymeric chain of PPy[22,23].

The morphologies of the products at different oxalic acid/pyrrole ratios were also examined. Fig. S1 (Supplementary Information) showed representative SEM images of the samples. All the SEM images illustrated hierarchical dendritic structures assembled with cauliflower-like structure of nanospheres, even though the oxalic acid/pyrrole ratio is 1/10. This demonstrates that oxalic acid plays an important role in the formation of hierarchical dendritic structure and cauliflower-like structure in PPy. When the oxalic acid/pyrrole ratio decreases up to 1, the numbers of the cauliflower-like structure in dendritic structure PPy relatively reduced (Fig. S1(a) and (b), Supplementary Information). With further decrease of oxalic acid/pyrrole ratio, the numbers of the cauliflower-like structure declined evidently and the spaces among dendritic structure were much greater (Fig. S1(c) and (f), Supplementary Information), and this phenomenon was further evidently presented when the oxalic acid/pyrrole ratio is 1/10 (Fig. S1(g) and (h), Supplementary Information).

It is proposed that oxalic acid induces the adsorption of pyrrole monomers onto its surface through intermolecular interactions such as hydrogen bonding and π-π interactions, and then pyrrole monomers were polymerized into PPy with cauliflower-like structure of nanosphere aggregates. The self-assembly of pyrrole via hydrogen bond and morphological evolution process of hierarchical dendritic PPy was illustrated in Schemes S1 and S2, respectively, Supplementary Information).

IR spectra of PPy and PPy$_{OA(3)}$ were characterized qualitatively in the range of 400-4000 cm^{-1} (Fig. 2). The results indicated that both PPy and PPy$_{OA(3)}$ samples possessed characteristic peaks of PPy: the absorption bands at 1558 cm^{-1} and 1477 cm^{-1} were individually attributed to the symmetric and asymmetric stretching vibrations of pyrrole ring, respectively[16]. The obvious peaks at 1203 cm^{-1} and 1313 cm^{-1} were associated with the C-N stretching in pyrrole rings of PPy backbones[17]. The broad band centred at 3426 cm^{-1} was assigned to the N-H stretching vibration in the pyrrole ring, while the relative absorption intensity at 1049 cm^{-1} and 929 cm^{-1} were proposed to be C-H in-plane deformation and C-H out-of-plane deformation, respectively[2425]. The upward peaks in IR between 1049 cm^{-1} and 929 cm^{-1} could imply the doping state of

polypyrrole[18]. All of these confirmed the formation of the PPy, however, the intensity of peaks for $PPy_{OA(3)}$ was relatively weaker than that for PPy. One possible explanation for this is that nanosphere aggregates in cauliflower-like structure of polymerized $PPy_{OA(3)}$ induced by oxalic acid affect the intensity of absorption band.

3.2. Electrochemical properties

Fig. 3 showed CV curves and corresponding galvanostatic charge/discharge (GCD) curves of PPy products with different nanostructures in 1 M H_2SO_4 electrolyte. As seen in Fig. 3(a), the CV curves for PPy samples deviated from ideal rectangular shapes, and displayed a pair of redox peaks, corresponding to the transition between oxidized and reduced PPy states[25], confirming involvement of pseudocapacitive charge storing mechanism. This was also confirmed by the GCD curves of PPy samples which are not ideally linear (Fig. 3(b)). Furthermore, it is interesting to note that, in the case of $PPy_{OA(3)}$ sample, the redox peaks (corresponding to a much higher current signal) in the CV curve were sharper than those for spherical PPy sample. It may be due to the fact that (1) better interaction of hierarchical dendritic $PPy_{OA(3)}$ with the electrolyte environment gives a more significant current signal owing to higher specific surface area than spherical PPy sample[26], and (2) the hierarchical dendrite structures provide easier path for ion and electron transmitting during charge/discharge process.

Moreover, $PPy_{OA(3)}$ sample possessed higher redox current density than spherical PPy sample at the same scan rate, indicating a much larger specific capacitance of hierarchical dendritic $PPy_{OA(3)}$. However, for $PPy_{OA(3)}$ sample and spherical PPy sample, there was no change in the anodic peak site and the cathodic peak site but the intensity of redox peaks for $PPy_{OA(3)}$ sample was relatively higher than spherical PPy sample, suggesting excellent interaction of $PPy_{OA(3)}$ with electrolyte because of fast diffusion and large electrochemical sites resulted from interconnected dendritic structures, as a result of the comparatively fast electrochemical response to the electrolyte. Furthermore, the CV curve area of dendritic $PPy_{OA(3)}$ sample was larger than that of spherical PPy sample, which demonstrated that the specific capacitance of $PPy_{OA(3)}$ sample was greatly improved owing to the larger surface area of hierarchical dendritic structure relative to micro-spherical grains. This is also confirmed by the GCD curves (Fig. 3(b)) and the specific capacitances of $PPy_{OA(3)}$ and PPy samples were 744 F/g and 309 F/g, respectively, according to the equation (1) (Table S1, Supplementary Information). To further verify the effect of oxalic acid/pyrrole ratio on the morphology of PPy, CV and GCD curves of PPy prepared at different oxalic acid/pyrrole ratios were conducted and shown in Fig. S2-3 (Supplementary Information).

CV curves of the $PPy_{OA(3)}$ electrode (Fig. 3(c)) presented approximately rectangular shape at the scan rate of from 5 mV/s to 100 mV/s, which suggesting the good pseudocapacitance performance with symmetrical redox behavior. The current density gradually increased with increasing scan rate, showing that the electrochemical process is diffusion-controlled[28]. Since the redox reactions involve doping and de-doping of ions from the electrolyte into the electrode, at lower scan rate, this implies that the ions can diffuse almost entirely into all the pores of the electrode.

GCD curves of the $PPy_{OA(3)}$ electrode at different current densities were shown in Fig. 3(d)), illustrating good symmetrical characteristic, which indicated that the hierarchical dendritic $PPy_{OA(3)}$ electrodes had excellent capacitive behavior and the redox process was reversible. Table 1 presented specific capacitances calculated by GCD curves at different current densities. It can be seen from Table 1 that hierarchical dendritic $PPy_{OA(3)}$ electrodes possessed a large specific capacitance as high as 744 F/g at a current density of 0.2 A/g and could achieve a higher specific capacitance of 362 F/g even at a current density of 5.0 A/g. The specific capacitance of the hierarchical dendritic $PPy_{OA(3)}$ electrode is better than some previous results such as PPy/carbon nanotubes nanocomposites-228 F/g at a current density of 0.5 A/g[29], PPy nanotubes-273 F/g at 0.5 A/g[30], and PPy nanowires-420 F/g at 1.5 A/g[15].

Electrochemical impedance spectroscopy (EIS) is a powerful and informative tool to evaluate the charge transport phenomena of materials[31]. The EIS data of all samples were analyzed via Nyquist plots consisting of three regions and shown in Fig. S4 (Supplementary Information), indicating that the electrode process is in the control of both charge transfer and diffusion processes[32,33]. The first part was an intercept at Z' axis in high frequency, and the second part was a semicircle in the middle frequency region, while the last part (the sloping line) was the Warburg impedance in the low frequency region. The impedance spectra presented in Fig. S5 (Supplementary Information) are fitted using the equivalent circuit model[34,35]. An intercept at Z' axis in high frequency corresponds to Ohmic resistance (R_Ω). The depressed semicircle in the middle frequency range is related to an interfacial charge-transfer process and its diameter directly correlates to the charge transfer resistance (R_{ct}). The low frequency Warburg impedance (Z_w) is ascribed mainly to the diffusion process of ions in the electrode[36-40].

The intercepts which correspond to the Ohmic resistance (R_Ω) were relatively small (about 0.75~2.5 Ω) (in Fig. S4, Supplementary Information) for all the plots, indicative of low inner resistance of both solution and electrode etc. Compared to spherical PPy with the complete larger semicircle which is indicative of the higher R_{ct}, the depressed semicircles of the plots for all hierarchical dendritic PPy samples were obviously observed and indicated lower R_{ct}. The lower R_{ct} could mainly be attributed to the facile electron transfer feasibility and good conductive nature of the dendritic PPy, which accelerate the electron transfer rate at the electrode surface, revealing a faster kinetics in electrochemical reactions. Moreover, the dendritic PPy products produce a large surface area on the electrode through the formation of the channel structure with their assembled cauliflower-like morphology, which facilitates the charge/electron transfer relative to the spherical PPy electrode. It implied that the hierarchical dendritic nanostructure could efficiently increase ionic conductivity which causes reduction in the electrode/electrolyte interface resistance[41].

As it can be seen in Fig. S4 (Supplementary Information), the slope of straight line for dendritic $PPy_{OA(3)}$ sample was less than 1, with the decline of oxalic acid content, the slope for PPy samples

Table 1. Specific capacitance of $PPy_{OA(3)}$ at different current densities

Current density (A/g)	0.2	0.4	0.6	0.8	1.0	2.0	5.0
Specific capacitance (F/g)	744	649	594	568	522	449	362

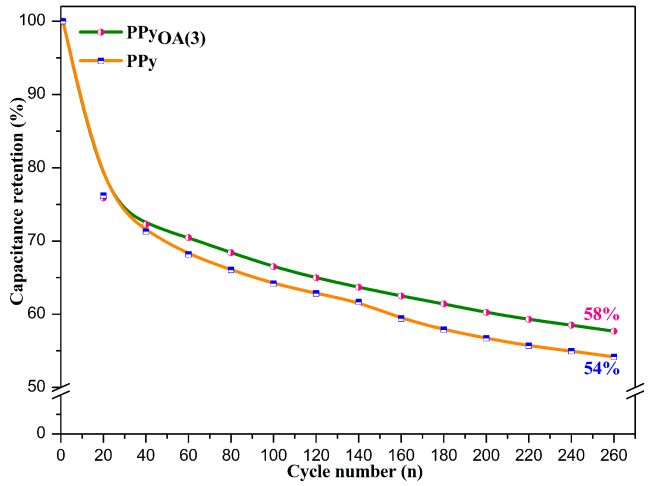

Figure 4. Capacitance retention of PPy and PPy$_{OA(3)}$ samples tested at scan rate of 10 mV/s.

gradually became larger and larger and the line was nearly parallel to the imaginary impedance axis (*Z″* axis) for spherical PPy without the presence of oxalic acid.

For ideal electrode process controlled by both charge transfer and diffusion process, the angle between the straight line and the X axis is 45°[42]. The plots showed an angle between 45° and 90° relative to the real impedance axis, displaying much shorter ions diffusion path and indicating the dominant diffusion control process of the electrode[43,44]. The angle deviated from 45° for dendritic PPy$_{OA(3)}$ sample reflected longer diffusion path of ions and increased obstruction of ion movement. It may be due to the fact that dendritic PPy$_{OA(3)}$ products with favorable interconnected pore structures were assembled with cauliflower-like structure of nanospheres, and the ions transferred among the pores, which prolonged the transmission path of ions relative to the dendritic PPy with sparse structures and spherical PPy with stacked and tight nanoparticles. However, the uniform interconnected pore facilitated the efficient access of electrolyte ions into the inside of electrodes, and the high specific surface area of dendritic PPy$_{OA(3)}$ ascribed to the interconnected pore structures could provide tremendous electrochemical sites for electrode/electrolyte contact[40], leading to the improvement of active material utilization and subsequent high specific capacitance. The capacitive behavior of PPy electrodes from the EIS is well consistent with the CV and GCD results.

Fig. 4 displayed the cyclic stability of the spherical PPy and dendritic PPy$_{OA(3)}$ electrodes investigated by continuous CV measurements over 260 cycles at the scan rate of 10 mV/s. The capacitance retention of the spherical PPy and dendritic PPy$_{OA(3)}$ electrodes had similar variation trend on the cycle number and were 58% and 54% retention of initial specific capacitance after 260 cycles, respectively. However, the initial specific capacitance of dendritic PPy$_{OA(3)}$ electrode was 2.4 times as much as that of spherical PPy electrode, suggesting that dendritic PPy$_{OA(3)}$ electrode still kept fairly high specific capacitance after 260 cycles. Compare to literature, capacitance maintained 55% at 10 mV/s for 5000 cycles[45], 60% at 2 mV/s for 5000 cycles[46], 50% at 25 mV/s for 500 cycles[47], 65.6% at 5 mV/s Forfor 10000cycles[48], 10% at 20 mV/s for 275 cycles[49]. conducting polymers, volume changes are often induced by the insertion and removal of counter-ions due to swelling and shrinking of electrode materials during the oxidation and reduction process, which causes the deterioration of cycle stability especially in the early process of circulation. It is a promising direction to prepare high-capacitance conducting polymers or their composites with withstanding severe volume changes.

4. CONCLUSIONS

In summary, polypyrrole with hierarchical dendritic structures assembled with cauliflower-like structure of nanospheres was successfully synthesized by chemical oxidation polymerization using oxalic acid as the template. The oxalic acid/pyrrole molar ratio has a significant effect on the formation of hierarchical dendritic structure and cauliflower-like structure in PPy. The hierarchical dendrite structures can provide not only better interaction with the electrolyte environment owing to higher specific surface area, but also easier path for ion and charge transfer during charge/discharge process. Therefore, the unique hierarchical dendritic structure endows PPy materials with a high specific capacitance of 744 F/g, which makes them have significant potential for the applications as promising electrode materials for high-performance supercapacitors.

5. ACKNOWLEDGEMENTS

This work was financially supported by NSFC (51363005), Guangxi Natural Science Foundation (2015GXNSFAA139277), Open Fund of Key Laboratory of New Processing Technology for Nonferrous Metal and Materials of Ministry of Education (14KF-1).

REFERENCES

[1] Y. Zhu, S. Murali, M. D. Stoller, K. J.Ganesh, P. Ferreira, R. M. Wallace, K. A. Cychosz, M. Thommes, E. A. Stach, R. S. Ruoff, Science, 332, 1537 (2011).
[2] Q. Chen, Y. Wang, T. Zhang, W. Yin, J. Yang, X. Wang, Electrochimi. Acta, 83, 65 (2012).
[3] J. Zhang, X. S. Zhao, The J. Phys. Chem. C, 116, 5420 (2012).
[4] Y. Liu, Y. Zhang, G. Ma, Z. Wang, K. Liu, H. Liu, Electrochimi. Acta, 88, 519 (2013).
[5] M. Li, J. Yuan, G. Shi, Thin Solid Films, 516, 3836 (2008).
[6] T. Patois, B. Lakard, N. Martin, P. Fievet, Synth. Met., 160, 480 (2010).
[7] J. H. Chang, C. R. Aleman de Leon, I. W. Hunter, Langmuir, 28, 4805 (2012).
[8] K. Li, H. Zhang, T. Tang, Y. Tang, Y. Wang, J. Jia, J. Power Sources, 324, 368 (2016).
[9] Y. He, S. Wang, J. Mu, L. Dai, Z. Zhang, Y. Sun, W. Shi, D. Ge, Materials Science and Engineering C, 71, 43 (2017).
[10]D.Wang, Y. X. Li, Z. Shi, H. L. Qin, L.Wang, X. F. Pei, J. Jin, Langmuir, 26, 14405 (2010).
[11]J. Lei, Z. Li, X. Lu, W. Wang, X. Bian, T. Zheng, Y. Xue, C. Wang, J. Colloid Interface Sci., 364, 555 (2011).
[12]H.Wang, C. Guo, S. Zhou, X. Hu, Y. Hu, F. Li, Y. Miao, Thin

Solid Films, 520, 2026 (2012).
[13]M. Onoda, K. Tada, A. Shinkuma, Thin Solid Films, 499, 61 (2006).
[14]X. Fan, Z. Yang, N. He, RSC Adv., 5, 15096 (2015).
[15]J. Zhao, J. Wu, B. Li, W. Du, Q. Huang, M. Zheng, H. Xue, H. Pang, Progress in Natural Science: Materials International, 26, 237 (2016).
[16]G. Wang, L. Zhang, J. Zhang, Chem. Soc. Rev., 41, 797 (2012).
[17]M. Mallouki, F. Tran-Van, C. Sarrazin, C. Chevrot, J.F. Fauvarque, Electrochim. Acta, 54, 2992 (2009).
[18] R. Li, Z. Chen, J. Li, C. Zhang, Q. Guo, Synth. Met., 171, 39 (2013).
[19]Z. X. Yu, Z. P. Yao, N. Zhang, Z. J. Wang, C. X. Li, X. J. Han, X. H. Wu, Z. H. Jiang, J. Mater. Chem. A, 1, 4571 (2013).
[20]C. Z. Wu, J. Dai, X. D. Zhang, J. L. Yang, Y. Xie, J. Am. Chem. Soc., 131, 7218 (2009).
[21]Y. Huang, X. F. Duan, Y. Cui, L. J. Lauhon, K. H. Kim, C. M. Lieber, Science, 294, 1313 (2001).
[22]M. Bazzaoui, L. Martins, E. A. Bazzaoui, J. I. Martins, Electrochim. Acta, 47, 2953 (2002).
[23]A. S. Liu, M. C. Bezerra, L. Y. Cho, Mater. Res. Ibero Am. J. Mater., 12, 503 (2009).
[24]G. Liu, H. Zheng, A. S. Simens, A. M. Minor,X. Song, V. S. Battaglia, J. Electrochem. Soc., 154, 1129 (2007).
[25]J. Huang, R. B. Kaner, Chem. Commun., 367 (2006).
[26]T. Tian, C. Zhang, W. Y. Hu, X. J. Kang, J. Yang, Z. Z. Gu, Anal. Meth., 5, 7066 (2013).
[27]D. P. Dubal, Z. C. Huertas, R. Holze, P. G. Romero, Electrochim. Acta, 191, 346 (2016).
[28]H. W. Park, T. Kim, J. Huh, M. Kang, J. E. Lee, H. Yoon, ACS Nano, 6, 7624 (2012).
[29]Y. Han, M. Shen, X. Lin, B. Ding, L. Zhang, H. Tong, X. Zhang, Synth. Met., 162, 753 (2012).
[30]J. G. Wang, B. Wei, F. Kang, RSC Adv., 4, 199 (2014).
[31]W. Sugimoto, H. Iwata, K. Yokoshima, Y. Murakami, Y. Takasu, J. Phys. Chem. B, 109, 7330 (2005).
[32]W. Fan, C. Zhang, W. W. Tjiu, K. P. Pramoda, C. He, T. Liu, ACS Appl. Mater. Inter., 5, 3382 (2013).
[33]M. D. Stoller, S. Park, Y. Zhu, J. An, R. S. Ruoff, Nano Lett., 8, 3498 (2008).
[34]X. P. Zhang, H. J. Guo, X. H. Li, Z. X. Wang, L. Wu, Electrochim. Acta, 64, 65 (2012).
[35]Z. Y. Chen, C. S. Dai, G. Wu, M. Nelson, X. G. Hu, R. X. Zhang, J. S. Liu, J. C. Xia, Electrochim. Acta, 55, 8595 (2010).
[36]D. Xu, Q. Xu, K. Wang, J. Chen, Z. Chen, ACS Appl. Mater. Inter., 6, 200 (2014).
[37] Z. Li, F. Du, X. F. Bie, D. Zhang, Y. M. Cai, X. R. Cui, C. Z. Wang, G. Chen, Y. J. Wei, J. Phys. Chem. C, 114, 22751 (2010).
[38]Y. Q. Qiao, J. P. Tu, X. L. Wang, C. D. Gu, J. Power Sources, 199, 287 (2012).
[39]J. Y. Xiang, J. P. Tu, L. Zhang, X. L. Wang, Y. Zhou, Y. Q. Qiao, Y. Lu, J. Power Sources, 195, 8331 (2010).
[40]D. Ghosh, S. Giri, M. Mandal, C. K. Das, RSC Adv., 4, 26094 (2014).
[41]B. C. Kim, W. J. Cho, W. G. Lee, S. J. Kim, R. Jalili, S. Y. Park, G. G. Wallace, K. H. Yu, S. J. Chang, Synth. Met., 193, 110 (2014).
[42]K. Zhang, L. L. Zhang, X. S. Zhao, J. Wu, Chem. Mater., 22, 1392 (2010).
[43]B. C. Kim, C. J. Raj, W. J. Cho, W. G. Lee, H. T. Jeong, K. H. Yu, J. Alloys Compd., 617, 491 (2014).
[44]C. J. Raj, B. C. Kim, W. J. Cho, W. G. Lee, Y. Seo, K.H. Yu, J. Alloys Compd., 586, 191 (2014).
[45]X. Lu, H. Dou, C. Yuan, S. Yang, L. Hao, F. Zhang, J. Power Sources, 197, 319 (2012).
[46]R. Xu, J. Wei, F. Guo, X. Cui, T. Zhang, H. Zhu, K. Wang, D. Wu, RSC Adv., 5, 22015 (2015).
[47]S. Huang, P. Chen, W. Lin, S. Lyu, G. Chen, X. Yin, W. Chen, RSC Adv., 6, 13359 (2016).
[48]Y. Zhou, X. Hu, Y. Shang, C. Hua, P. Song, X. Li, Y. Zhang, A. Cao, RSC Adv., 6, 62062 (2016).
[49]Y. J. Peng, T. H. Wu, C. T. Hsu, S. M. Li, M. G. Chen, C. C. Hu, J. Power Sources, 272, 970 (2014).

Supplementary Information

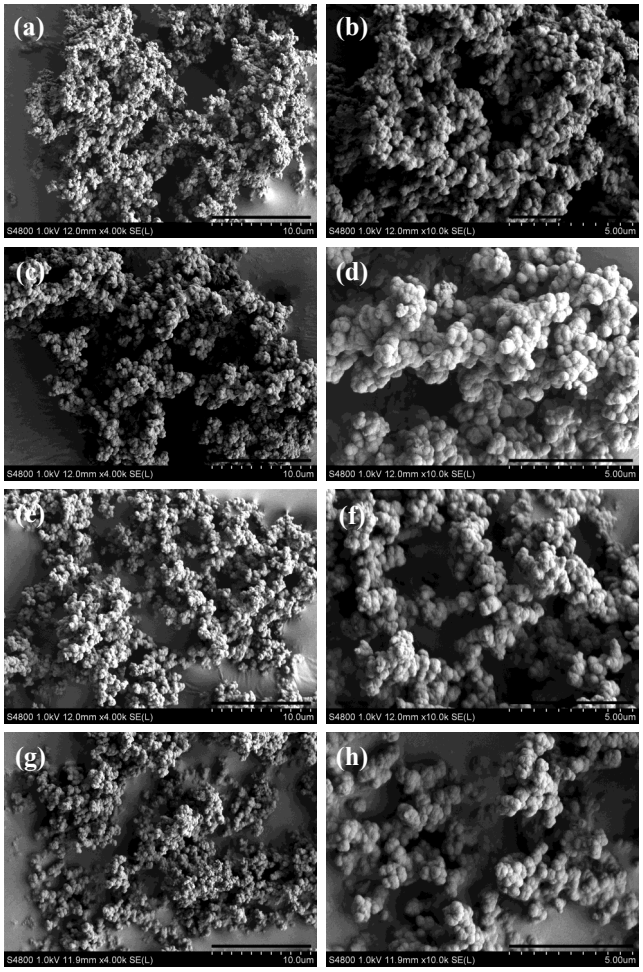

Fig. S1. SEM images of (a,b) $PPy_{OA(1)}$, (c,d) $PPy_{OA(1/3)}$, (e,f) $PPy_{OA(1/5)}$ and (g,h) $PPy_{OA(1/10)}$ samples.

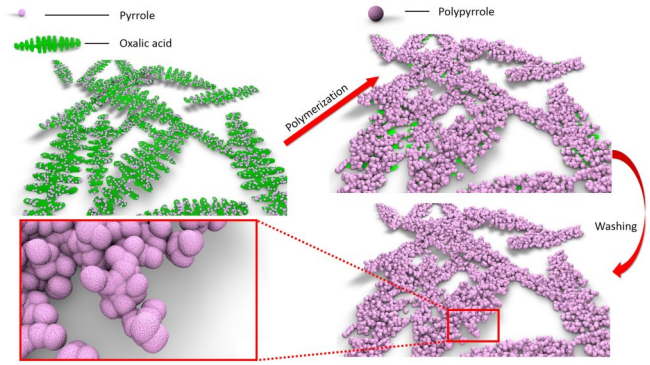

Scheme S2. Schematic illustration of the synthesis of hierarchical dendritic polypyrrole

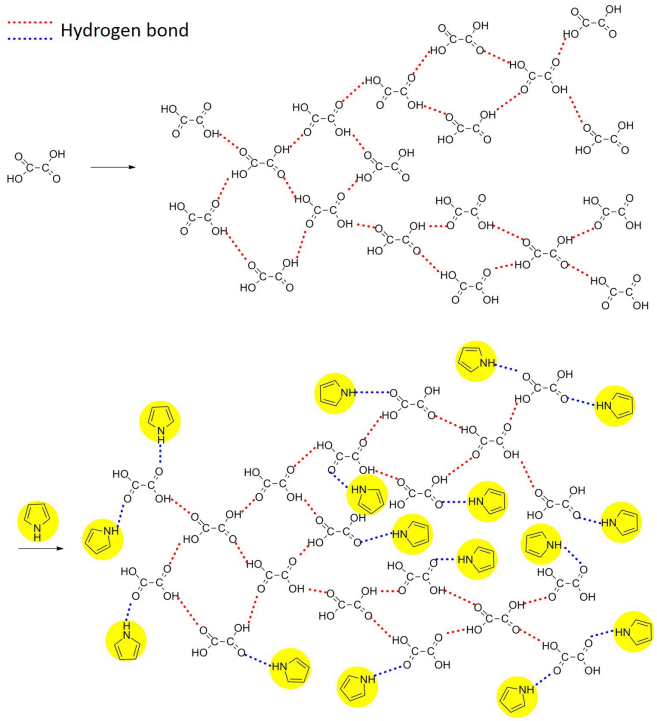

Scheme S1. Schematic diagram of self-assembly of pyrrole via hydrogen bond.

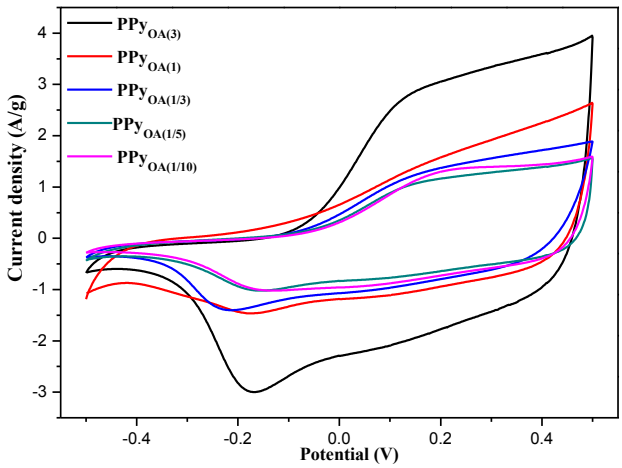

Fig. S2 CV curves of dendritic PPy samples at scan rate of 5 mV/s(vs. SCE).

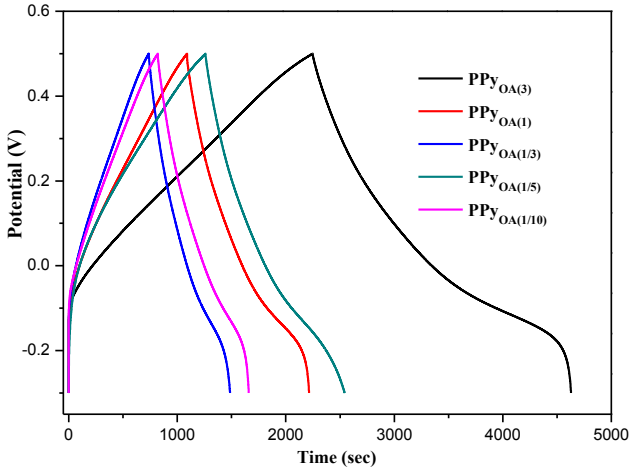

Fig. S3. GCD curves of dendritic PPy samples at current density of 0.2 A/g.

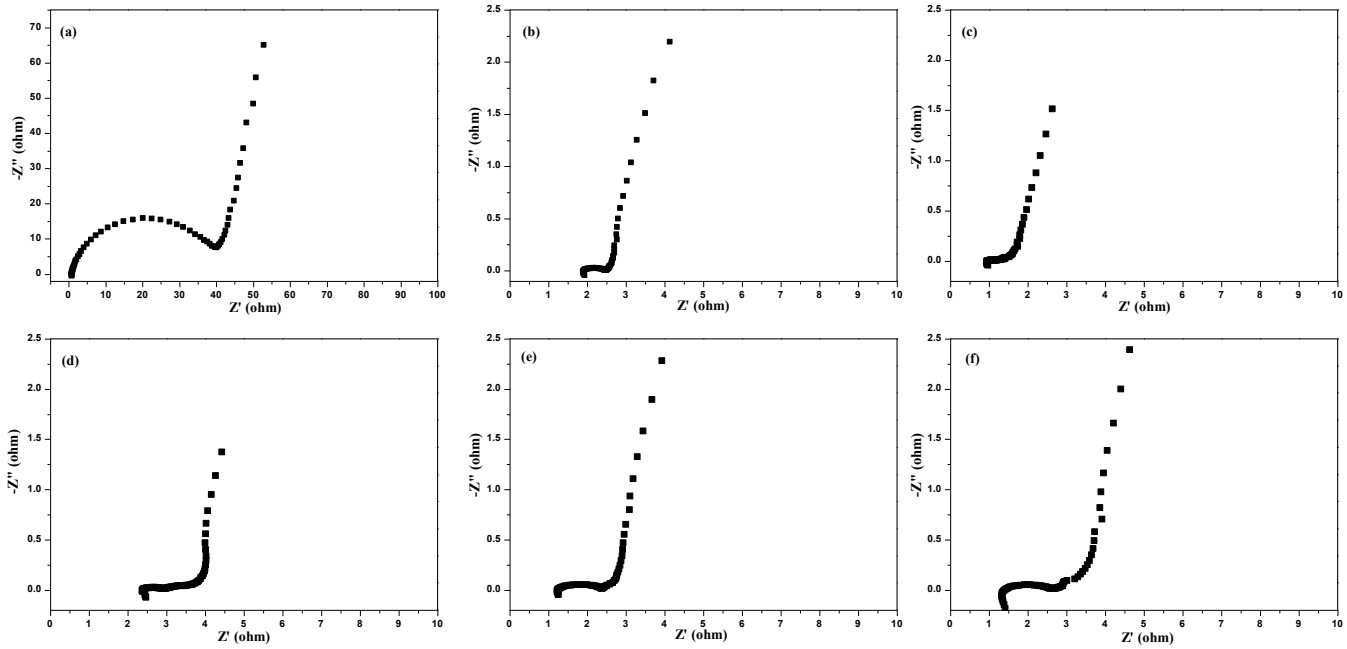

Fig. S4. Nyquist plots of (a) PPy, (b) $PPy_{OA(3)}$, (c) $PPy_{OA(1)}$, (d) $PPy_{OA(1/3)}$, (e) $PPy_{OA(1/5)}$ and (f) $PPy_{OA(1/10)}$ at scan rate of 10 mV/s.

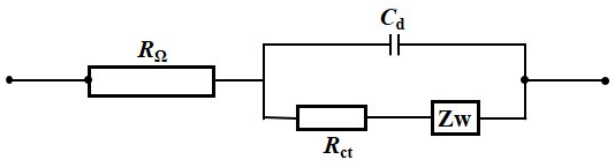

Fig. S5. The equivalent circuit model for PPy electrodes.

Table S1. Specific capacitance of dendritic PPy materials at current density of 0.2A/g

sample	PPy	$PPy_{OA(1/10)}$	$PPy_{OA(1/5)}$	$PPy_{OA(1/3)}$	$PPy_{(OA(1)}$	$PPy_{(OA(3)}$
Specific capacitance (F/g)	309	262	233	352	401	744